Photoionization of silicon particles in SiO_2

V. V. Afanas'ev and A. Stesmans
Laboratory of Semiconductor Physics, University of Leuven, Celestijnenlaan 200 D, 3001 Leuven, Belgium
(Received 30 October 1997; revised manuscript received 2 March 1998)

The density of electron states of nm-size Si particles in SiO_2 layers produced by implanting O^+ ions into Si is analyzed using a newly developed total optical depopulation technique. The distribution of states is found to be indistinguishable for neutral and negatively charged particles, and nearly independent of the particle size. This indicates that the optical excitation is related to defects in the oxide surrounding the particles. Two components of the defect spectrum are isolated, both related to the Si enrichment of the oxide, with energy levels at 2.8 and 3.1 eV below the SiO_2 conduction band. The latter is related to the H-complexed O vacancy in SiO_2 and its contribution is significantly enhanced upon hydrogenation. Electron states originating from quantum confinement in Si particles are observed only in the smallest Si clusters; in all other cases electrons are found to be trapped in the oxide. The blue luminescence, known for the oxidized Si particles, may be consistently explained from the obtained electronic spectra suggesting the charge transfer between a Si particle and neighboring oxide defects as a feasible mechanism. [S0163-1829(99)06003-8]

I. INTRODUCTION

Silicon clusters embedded in SiO_2 attract considerable interest because, like porous Si, they exhibit efficient photoluminescence (PL) without, however, pronounced aging effects.[1–4] Moreover, the oxide present on the Si particle surface leads to blue-green[5–8] and ultraviolet (UV) PL,[9–11] in contrast with porous Si where the PL is typically in the red-orange spectral range.[1,4,12–14] Together with the observation of different luminescence dynamics (the blue-green band decays much faster than the red-orange one[3,5]), the correlation between the short-wavelength PL and the presence of Si-O bonds[3] led several authors to suggest that there is a luminescence mechanism related to the coverage of the Si particles with oxide.[3,4,7,13,14] It is worth mentioning here that a recent review[14] indicated that the fast blue-green and UV PL are *only* observed from oxidized porous Si layers. Therefore, in addition to the quantum confinement effect which affects the spectrum of electron states in the Si core,[13,14] there is an Si/oxide interface-related component of electron states prone to efficient optical excitation and/or radiative recombination. These are at the basis of the blue PL, with an efficiency as high as 0.1%.[3] Indeed, the blue PL from oxygen deficient silica is well known.[15–19] It is believed to be related to the intrinsic oxide defects: the diamagnetic oxygen vacancy ($O_3{\equiv}Si{-}Si{\equiv}O_3$) (Refs. 16, 20–23) or the twofold coordinated Si center (O-Si-O).[18,24] At first, one might expect the presence of Si-enriched oxide at the Si/oxide interface, that may contain a high concentration of such centers. Efficient PL may be pictured in this case as occurring in three stages: light absorption in the Si core, transfer of the electronic excitation to the Si particle/oxide interface, and radiative recombination at the interfacial defect.[25,26] This scenario, though intuitively acceptable, faces the problem that both the neutral O vacancy[27–29] and twofold coordinated silicon[29] have their energy level E_t of the negatively charged state only slightly below the SiO_2 conduction band edge [$E_C(SiO_2)-E_t \sim 1$ eV], i.e., they cannot directly trap an electron from the conduction band of Si. The bottom of the latter band lies at 3.2 eV below $E_C(SiO_2)$ at the bulk Si/SiO_2 interface,[30] and expecting it to be shifted ~2 eV upwards is unrealistic in a view of the shift of only ~1–1.5 eV of the optical absorption edge measured in porous Si upon reduction of the crystallite size.[1,31,32] At the same time, the Si/SiO_2 interfaces typically have a low density of interface states with energy levels in the Si bandgap (down to the range of 10^{10} cm^{-2} eV^{-1}) (Ref. 33), which cannot account for the efficient short-wavelength PL. Consequently, either defects of other types must be present at the interface,[34,35] or else, the PL of Si particles is due to an excitonic state[36] of which the PL spectrum incidentally coincides with the SiO_2 PL.

In the present work evidence will be presented for the feasibility of the defect-mediated blue PL mechanism. We have attempted to analyze the energy spectrum of electron states of Si particles in SiO_2 in a most straightforward manner, i.e., by photoexciting the particles from the neutral to the positively charged state [photoionization (PI)] or from the negative (upon capturing an electron) to the neutral state [photoneutralization (PN)]. We found that both PI and PN occur by mediation of the optical excitation of oxide defects at the Si core/SiO_2 interface indicating a transfer of the optically excited (PI) or trapped (PN) electrons to the energy levels of these defects. Also, there is significant energy redistribution of these states upon annealing in H_2, suggesting one of the states to be the hydrogen-complexed oxygen vacancy center. This suggestion is confirmed, in combination with electron spin resonance (ESR) analysis, by the generation of photoactive electron traps with similar energy spectrum in stoichiometric SiO_2 under heavy irradiation with 10 eV photons. Therefore, we conclude that electron trapping by near-interfacial defects in SiO_2 may be involved in the highly efficient short-wavelength PL of oxidized (SiO_2 covered) Si particles.

©1999 The American Physical Society

TABLE I. Sample parameters and properties of Si particles in the oxide.

Type	O^+ dose (10^{18} cm^{-2})	Oxide thickness (nm)	N ($\pm 10\%$) (10^{12} cm^{-2})	σ ($\pm 20\%$) (10^{-14} cm^2)	r_c ($\pm 10\%$) (nm)
A	1.54–1.8	320–360	2.5–3	20	2
B	1.7	340	3.5	40	3
C	1.7	330	1.5	5	1
D	(0.5+0.5+0.8)	360	0.7	1	0.5
E	0	36–400	0		

II. EXPERIMENT

A. Sample preparation

There exists a variety of methods to produce Si particles with SiO_2 overlayer, such as oxidation of porous Si,[1–7,13,37] Si nanoclusters,[8,36] thin Si overlayers,[38,39] Si^+ ion implantation into SiO_2 (Refs. 40–46), O^+ ion implantation into Si,[47–49] deposition of Si-enriched oxides,[50–54] and epitaxial Si growth under simultaneous O^+ ion implantation.[55] These systems typically show PL in the red-infrared ($h\nu = 1.4-1.7$ eV), blue-green ($h\nu = 2.2-2.7$ eV), and UV ($h\nu = 4.2-4.4$ eV) spectral ranges, with a good agreement between the different preparation methods thus pointing to common radiative channels. Therefore, we used only one technique to produce SiO_2 containing Si particles: implantation of O^+ ions into (100)Si substrates followed by high-temperature (1320–1350 °C) post-implantation annealing. It provides several advantages for physical characterization: (i) the buried SiO_2 layers have good insulating properties in terms of electrical breakdown field and conductivity.[56] This allows charging of Si particles in the oxide and keeping them in this state;[47] (ii) the SiO_2 layer containing Si particles is formed on high-quality Si substrates with the oxide/substrate interface defect density typically below 3×10^{10} cm^{-2}. This allows one to measure the sign and the density of electrical charge related with Si particles using the capacitance-voltage (C-V) technique;[33] (iii) the presence of the superficial Si layer prevents diffusion of foreign atoms into the buried oxide, particularly hydrogen. This enabled us to isolate the effect of H on the electronic spectrum by comparing as-prepared SiO_2 layers with those intentionally annealed in H_2.

The studied samples, supplied by three independent industrial vendors, were prepared by implanting O^+ ions into low doped n/p-type (100)Si wafers. The O^+ implantation dose and ion energy were in the range $(1.54-1.8)\times10^{18}$ cm^{-2} and 160–210 keV, respectively. Subsequent annealing at 1320–1350 °C in Ar+0.5% O_2, resulted in the formation of buried oxide (BOX) layers with thicknesses of 320–360 nm. More details on sample preparation and the oxide microstructure were published elsewhere.[57,58] Important for the present study is that the variation in the O^+ implantation mode causes drastic changes in the density and size of Si particles embedded in the buried SiO_2 layer. This was suggested to be related to the pressure-driven formation of a densified crystalline SiO_2 polymorph, which prevents outdiffusion of Si from the oxide.[59] We will present results for four types of samples (labeled $A-D$) that provide us with a set exhibiting a monotonic variation in the average size of Si inclusions down to nm-sized Si clusters, undetectable by transmission electron microscopy (TEM). The samples A-C were prepared by a single step implantation of $(1.5-1.8)\times10^{18}$ O^+/cm^2 with the wafer being rotated during implantation (*A*), and the wafer fixed in a channeling (*B*) and nonchanneling (*C*) orientation with respect to the O^+ ion beam. Another set of samples type *C* was obtained using randomization of the O^+ ion beam by a screen SiO_2 layer, deposited onto Si surface prior to implantation.[58] The samples of type *D* were prepared by triple implantation $(0.5+0.5+0.8)\times10^{18}$ O^+/cm^2 with additional anneals between the steps. The samples of type *E* were prepared by conventional thermal oxidation of (100)Si at 1000 or 1350 °C; these oxides contain no Si particles. The sample parameters are summarized in Table I.

After the sample preparation, the top Si layer was removed by wet etching and replaced by semitransparent Al or Au electrodes of 0.5 mm^2 area evaporated from a resistively heated source. Some of the samples were annealed in H_2 (1.1 atm, 1100 °C, 1 h) prior to metalization. The nonmetalized samples of types *A, D*, and *E* were analyzed by the electroluminescence (EL) technique.[48] The first two samples show blue ($h\nu = 2.6-2.7$ eV) and UV ($h\nu = 4.2-4.3$ eV) EL, matching with that known for Si particles in SiO_2.[60] The intensity of the blue EL in these samples is $\sim10^3$ times higher than in the particle-free samples *E*. The samples were also analyzed by *K*-band ESR at 4.3 K as described elsewhere.[61]

In order to estimate the size of Si particles, the oxides were examined by transmission electron microscopy and atomic force microscopy (AFM) as described elsewhere.[58,59] TEM shows the presence of platelet-shaped c-Si islands near the Si-substrate/BOX interface. They exhibit a broad size distribution: 40–200 nm across and 20–40 nm thick in samples type *A*, and up to 300 nm across and 30–40 nm thick in samples type *B*; No c-Si inclusions could be distinguished in samples *C* and *D*. AFM images of the substrate after oxide etching in aqueous HF reveal inhomogeneities with a considerably reduced etch rate, which were found to consist of Si particles and a densified SiO_2 phase (coesitelike).[58,59] However, comparison between AFM images and TEM data, importantly, shows that ~90% of the etching inhomogeneities in AFM images do not provide a distinguishable c-Si diffraction contrast in the TEM observations.[58] Most indicative for this discrepancy here is the AFM observation of the inhomogeneities of smaller size in samples *C* and *D* in which TEM fails to observe any c-Si islands. Apparently, the vast majority of Si inclusions are either too small or their crystalline structure is too distorted to provide any contrast distinguishable on the background of

electrons scattered by the surrounding SiO_2. Obviously, neither TEM, which reveals only the largest c-Si inclusions, nor AFM, which is unable to discriminate between Si inclusions in slowly etching SiO_2, can serve as a reliable tool for the determination of the Si particles size. Therefore, we employed a different physical principle to characterize Si inclusions in the oxide. It is based on the fact that a Si particle imbedded into SiO_2 constitutes a potential well for electrons from the oxide conduction band. Consequently, electrons injected into the SiO_2 layer will be trapped by these Si inclusions, thus generating negative fixed charge in the oxide layer. As the probability of the trapping event is proportional to the size of Si inclusion, the latter can be estimated from the negative charging kinetics. Here, it is important to add that these deep electron traps can be related only to an inclusion of Si, not to an inclusion of a different SiO_2 polymorph, however. This approach will be discussed in more detail in the next section.

B. Photoionization and photoneutralization spectroscopy: Total optical depopulation technique

The routine way to investigate the depopulation of electron states consists of measurement of the photocurrent related to their photoexcitation as a function of the photon energy.[62–65] However, because the photocurrent is proportional to the convolution of the density of states (DOS) available for depopulation and the energy-dependent photoionization cross section (σ_{ph}), the photocurrent monitoring, in general, is unable to provide the DOS in a straightforward way. Therefore, we developed an approach employing the measurement of the oxide charge variation upon optical excitation: The determination of the energy spectrum of Si particles in SiO_2 is based on the optical excitation of electron transitions from the populated states of the Si particles to the oxide conduction band. These transitions alter the charge state of the particles that is detected by the C-V technique.

We used a total (exhaustive) depopulation of the traps in incremental narrow spectral windows. As a result, the DOS available for PI/PN in each energy window (corresponding to the increase of $h\nu$) is directly determined, while the corresponding σ_{ph} can be obtained from the depopulation kinetics at each photon energy. There is, however, an uncertainty in assigning the photon energy at which depopulation is observed, i.e., determining the ionization energy of the trap $E = E_C(SiO_2) - E_t$. The reason is that the depopulation is related to the power dependence of σ_{ph} on the photon energy $\sigma_{ph} \sim (h\nu - E)^p$ at $h\nu \geqslant E$,[66,67] which gives $\sigma_{ph} = 0$ at $h\nu = E$. Consequently, the photon energy at which an efficient depopulation is observed will be always larger than E, thus causing a systematic shift of the DOS distribution. In order to minimize this shift, the time allowed for detrapping was kept long enough to allow nearly exhaustive photoionization of states in the vicinity of their photoionization threshold. We will show below that the maximal shift of the DOS in our experiments does not exceed 200 meV.

The PI measurements were performed using the spectral system described previously.[68] The samples were biased by applying a potential to the metal electrode to create an electric field F in the oxide of 0.3, 0.5, or 1.0 MV/cm (no substantial impact of the applied potential polarity on the depopulation was observed). Prior to illumination, the samples were aged for $\sim 10^5$ s in darkness, and then exposed to monochromatic light with the photon energy increasing from 1.7 to 5.5 eV. The spectral resolution was kept constant (6 nm) and the measurement time per spectral step was 100–110 min for the total depopulation and 20–30 s for the yield measurements, during which 1 MHz C-V curves were recorded. All measurements were performed at room temperature.

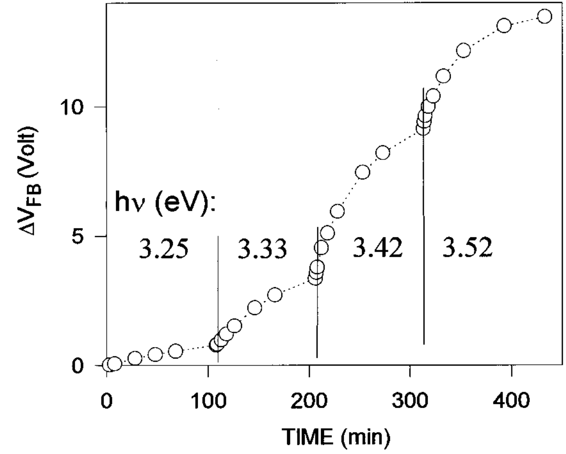

FIG. 1. Shift of the C-V curve flatband voltage in sample type A during photoionization as a function of the illumination time. The photon energy $h\nu$ increases from 3.25 to 3.52 eV in ~0.1-eV steps.

An example of how the total PI curve (transition from the neutral to the positive state) is obtained by monitoring the shift of the flatband point (V_{FB}) on the C-V curve is shown in Fig. 1 for sample A. After each increment in $h\nu$, the depopulation was traced for 100–110 min to ensure that 80–90 % of the photoactive defects had changed their charge state. The DOS, measured with respect to $E_C(SiO_2)$, is calculated for each energy window from the charge density obtained from the V_{FB} shift[33] normalized to the width $\delta(h\nu)$ of the corresponding energy interval, given as $D_t = \Delta V_{FB} C_{OX} / q\delta(h\nu)$, where q is the elemental charge, and C_{OX} is the specific capacitance of the oxide layer. Because the *saturation* of the detrapping curve is the only criterion employed, the obtained DOS requires no correction for the spectral distribution of the light source or top electrode transparency, optical interference in the oxide layer, etc., thus providing most reliable physical information. The σ_{ph} value at each energy was determined by fitting first-order kinetics using the photon flux penetrating the metal electrode, measured independently on coprocessed metalized quartz window samples. Each σ_{ph} value relates only to the states depopulated in the corresponding narrow energy range, because almost all the states with lower photoionization energy were already emptied previously.

The PI/PN was also analyzed in a quantum yield (Y) mode, that is, under conditions of a small change in the population of electron states. It was done by measuring the shift of the C-V curve after short (20 s) light exposure and normalizing the charge density variation to the photon flux n_{ph}: $Y = \Delta V_{FB} C_{OX} / q n_{ph}$. In contrast with the total depopulation mode, all the states with the photoionization thresholds satisfying $E_C(SiO_2) - E_t < h\nu$ contribute to the

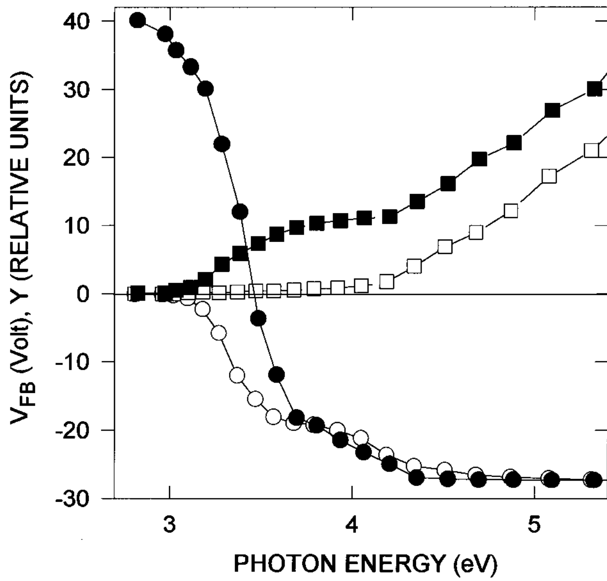

FIG. 2. C-V curve flatband voltage (circles) and quantum yield (squares) of photoionization (open symbols) and photoneutralization (filled symbols) measured in sample type A as a function of the exciting photon energy.

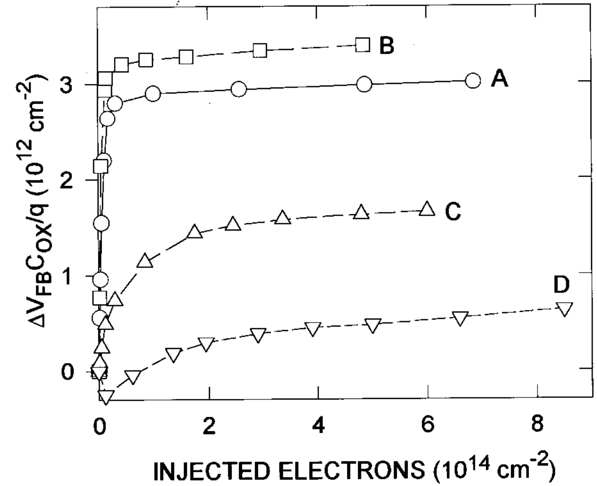

FIG. 3. Effective density of trapped negative charge in samples $A-D$ determined from the C-V curve shift as a function of density of electrons injected into the oxide.

yield. The difference between the total depopulation and the yield modes of PI/PN measurements is illustrated in Fig. 2, showing for sample A the C-V curve shift and the yield for both PI (open symbols) and PN (filled symbols) as a function of the photon energy. The total depopulation curve indicates that nearly all the available states are ionized or depopulated in the spectral range of $3<h\nu<4$ eV. In contrast, the yield is low in this spectral range, particularly for PI, but it increases steeply at $h\nu>4.3$ eV. Obviously then, the increase in Y indicates an enhancement of the σ_{ph}, but not the onset of a high density of new states available for depopulation.

Prior to PN measurements, electrons were injected into the oxide to fill the traps, which occurs most efficient for Si inclusions.[47,57,58] The injection was periodically interrupted to record the C-V curve from which the density of trapped electrons was determined. An example of the electron trapping kinetics is shown in Fig. 3 for samples $A-D$. The specimens exhibit a large variation in the total density of trapped electrons which reflects a different density of Si particles included in the oxide (N). The inferred values are listed in Table I. The thermal SiO_2 layers, free of Si inclusions, show no significant electron trapping in the covered range of the injected electron density. Analysis of the trapping curves using the algorithm of Ning[69] bears out a variation in the capture cross section (σ) of the dominant electron traps from 1×10^{-14} cm^2 in sample D to 4×10^{-13} cm^2 in sample B. This refers to a different capture radius of the traps, which can be estimated[70] as $2r_c\approx(\sigma)^{1/2}$. As σ is found to be independent of the electric field strength in the oxide,[47] the obtained value of r_c will be proportional to the geometric radius of the trapping Si particle, i.e., the size of the largest Si clusters available in a given sample. The thus inferred r_c values are also listed in Table I together with the measurement errors reflecting the data scattering. As to the absolute accuracy, the physical accuracy of this method is basically governed by the assumption that the trapping event occurs if an electron enters the Si particle. In a more complete picture, though, the trapping requires an additional stage, i.e., inelastic scattering of the electron inside the particle, which may cause the inferred capture radius to deviate from the true particle radius. The inelastic scattering event probability can be calculated as $[1-\exp(-2r_c/l)]$ (Ref. 71) where we may take $l\approx1$ nm for the photoelectron inelastic scattering length.[72] For the smallest particles (in sample D), $r_c\approx0.5$ nm yielding a scattering probability of 0.63. With $r_c=1$ nm (sample C) the scattering probability increases to 0.86, i.e., the inaccuracy linked with the basic assumption becomes smaller than the measurement error (20%). Obviously then, for particles of larger size (samples A,B) the capture and geometrical radii of the particle will coincide, with reliable r_c values as a result. The data listed in Table I importantly indicate that for a fixed number of injected electrons, for each sample type, particles of different size are automatically selected, and, in the course of PN experiments, the DOS of only these particles is analyzed. For the present work, we fixed on an injection at 2×10^{14} electrons/cm^2 at $F=1$ MV/cm, the metal being negatively biased.[47,57,58,70] Subsequently, the samples were aged and analyzed in the same way as in the course of PI experiments.

III. RESULTS

A. DOS determined from PI and PN experiments

The DOS distributions determined from the total depopulation PI (dashed curves) and PN (dotted curves) are compared in Figs. 4(a)–(d) for the samples $A-D$, respectively. The origin of the energy scale is put at the bottom of SiO_2 conduction band. The main observations are as follows: (i) No PI/PN is observed in the particle-free samples type E, in contrast with samples $A-D$. This importantly demonstrates PI/PN to be related with the Si particles. (ii) The PI and PN DOS typically show two 0.2–0.4 eV-wide DOS bands around $E\sim3.5$ and ~4.5 eV. (iii) With reduction of r_c (see Table I), the DOS exhibits two trends: (1) the PI becomes less efficient and (2) the PI band at $E\sim4.5$ eV increases rela-

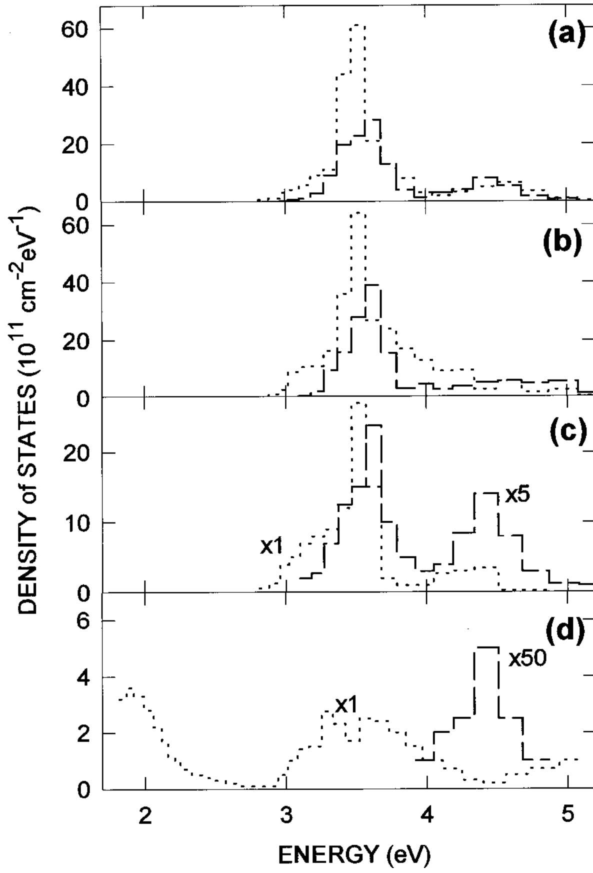

FIG. 4. Density of states in samples $A-D$ [(a)–(d), respectively] determined from PI (dashed line) and PN (dotted line) as a function of energy *below* the SiO_2 conduction band.

tively to the PI/PN band at $E\sim3.5$ eV. (iv) There is no shift in the DOS that might be associated with the decrease in Si particle size. (v) In samples $A-C$, the DOS determined from PI and PN experiments are nearly identical; there is only some scaling and a global shift of the PI DOS by 200–300 meV. (vi) In sample D, the PI exhibits only one weak band at $E\sim4.5$ eV, while the PN shows the $E\sim3.5$ eV band, similar to that in samples $A-C$, and a band of shallow traps at $\sim$2 eV.

To ensure that the observed PN spectra are related to the excitation of the Si particles that have trapped an electron, and not to the PI of neighboring neutral particles leading to charge compensation, we repeated the electron injection upon reaching $V_{FB}=0$ (cf. Fig. 2). Analysis of the electron retrapping kinetics gave the same σ values as in the course of first electron injection. Therefore, it is concluded that the PN provides the DOS of the negatively charged Si clusters.

The positively charged state of the Si particles observed after PI was analyzed by electron spin resonance (ESR). We found no paramagnetic states despite the high density of positively charged centers. However, an intense E'_γ signal originating from oxygen vacancies ($O_3\equiv Si\cdot$ center, where the dot symbolizes an unpaired electron) is observed upon hole injection into the SiO_2.[58] From this, we conclude that the positive charge introduced during PI is likely localized on the Si particles, but not on the SiO_2 defects, i.e., there is no transfer of holes from the Si clusters into the oxide.

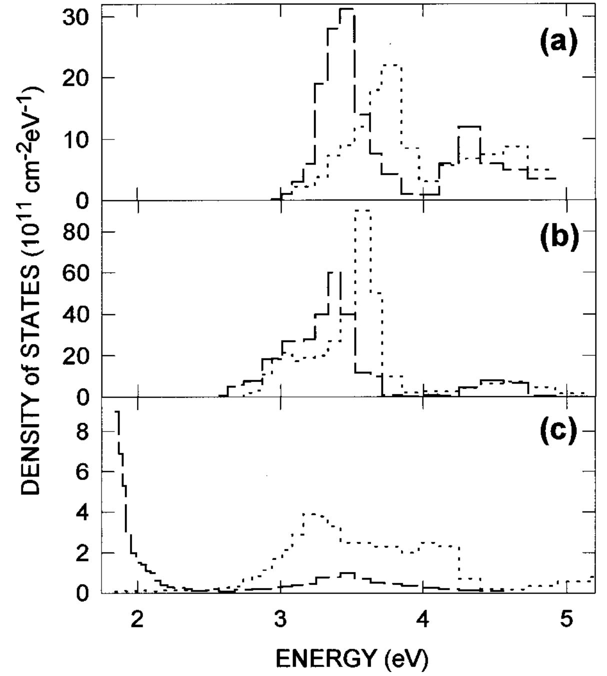

FIG. 5. Density of states in control (dashed line) and hydrogenated (dotted line) samples determined from PI (a) and PN (b) in sample A and from PN in sample D (c) as a function of energy *below* the SiO_2 conduction band.

B. Effect of hydrogenation on DOS

The DOS distributions are shown in Fig. 5 for samples A (a,b) and D (c) as determined from the PI (a) and PN (b,c) in the untreated state (dashed curves) and after annealing in H_2 at 1100 °C (dotted curves). In sample A the hydrogenation is seen to result in a redistribution of the DOS in the 3.5 eV band by shifting its center of gravity $\sim$300 meV away from $E_C(SiO_2)$. At the same time, the onset of the PI/PN DOS curves remains unchanged within an accuracy of 50 meV. This behavior suggests a complex nature of the DOS band, exhibiting, among others, low-energy states barely affected by H, and deeper states created upon H_2 annealing. Hydrogenation of sample D has a dramatic effect on the PN DOS: its shallow portion is eliminated and a 1-eV-broad, apparently two-component band appears at around 3.5 eV. The latter resembles the PN DOS of the hydrogenated sample A, which may point to the same type of the H-generated defects. Upon hydrogenation, sample D additionally shows a significant portion of optically inactive electron traps, i.e., those which cannot be optically discharged.

The dependence of σ_{ph} on the *trap energy* (not to be mixed with the dependence of σ_{ph} on $h\nu$) was inferred from the kinetics of PI and PN (not shown). The states observed at $E\sim2$ eV with PN on sample D exhibit a large σ_{ph} ($3-6\times10^{-18}$ cm^2) as compared to the states distributed in the 3–4 eV range ($\sigma_{ph}=0.7-1.5\times10^{-18}$ cm^2), which may refer to a difference in atomic structure. The cross section of PI, in turn, is lower than that for PN, which may be due to a different initial charge state of the center. In the energy range of $3<h\nu<4$ eV, σ_{ph} of both PI and PN show no substantial variation: most of the excited states have a similar σ_{ph}. However, σ_{ph} decreases by approximately 50% upon hydrogenation, which may be due to a structural change of the photoactive state.

C. Optical excitation of SiO_2 defects

In order to get insight into the nature of the states contributing to the DOS of Si particles in SiO_2, we separately studied optical excitation of electrons from the oxide defects present at the Si/SiO_2 interface and defects generated in the bulk of the oxide of sample type *E*. A first result concerns our previous work, revealing the presence of near-interfacial oxide defects which can trap electrons from Si in a level 2.8 eV below $E_C(SiO_2)$, as determined by the photon-stimulated electron tunneling (PST) and photoexcitation of the electrons into the oxide conduction band.[73–75] The density of these defects is found to be substantially higher in the samples of type *A* and *B* than in samples *C* and *D* (cf. Fig. 3 in Ref. 74), i.e., it likely correlates with the presence of Si particles in the oxide. This result suggests the possible involvement of the 2.8 eV defect level in the PI/PN studied in the present work. This supposition is supported by the buildup of positive charge in samples $A-C$ with densities reaching 2×10^{12} el.charges/cm^2 and the elimination of negative charge in samples $A-D$ observed under conditions of PST (excitation with an Ar^+ ion laser at $h\nu = 2.71$ eV). It can also be seen from Figs. 4 and 5 that the energy onset of the PN DOS is in the range of 2.8–3.0 eV, that is, at nearly the same energy level as of the above discussed defects. Besides the independent affirmation of the trap energy level, this result assures the reliability of the DOS energy scale within 200 meV.

Second, we also found previously that irradiation of a defect-free SiO_2 with 10-eV photons generates a large concentration ($>10^{19}$ cm^{-3}) of electrically neutral E'_γ centers, which is pictured as removal of an O atom from a Si-O-Si bridge towards an interstitial position followed by decoration with hydrogen (see Ref. 61 for details). There are two important observations pertinent to the present study: (i) the intense ESR signal from the E'_γ center (see Fig. 9 in Ref. 61) disappears upon hydrogenation (1.1 atm H_2, 400 °C, 30 min), but can be restored by hole injection indicating reversible switching between the paramagnetic ($O_3\equiv Si\cdot\ HSi\equiv O_3$) and the diamagnetic ($O_3\equiv SiH\ HSi\equiv O_3$) states; (ii) the electrons trapped by the irradiation-generated defects may be optically detrapped both in the paramagnetic and H-passivated diamagnetic state. The latter is illustrated by Fig. 6 in which the photocurrent per incident photon is shown as a function of photon energy for the control sample (type *E*) with 66-nm-thick oxide, the same sample exposed to 10^{19} 10-eV photons/cm^2, and after hydrogenation at 400 °C. All the curves are measured with an applied $F = 4$ MV/cm, the metal being positively biased, to inject electrons from Si into the defects located in the near-interfacial SiO_2 layers. In the control sample, a first observation is the intense internal photoemission of electrons from the Si substrate valence band: It is characterized by $Y \sim (h\nu - \Phi_0)^3$ and a field-*dependent* (the Schottky effect) spectral threshold Φ_0, which, when extrapolated to zero field, gives the barrier height of $(4.25 \pm 0.05$ eV), the value characteristic for electron emission from the Si valence band to the SiO_2 conduction band.[30,76] Second, there is a much weaker emission, characterized by $Y \sim (h\nu - \Phi_1)$ and the field-*independent* spectral threshold $\Phi_1 = (2.8 \pm 0.1)$ eV, which, as we discussed in the previous paragraph, is related

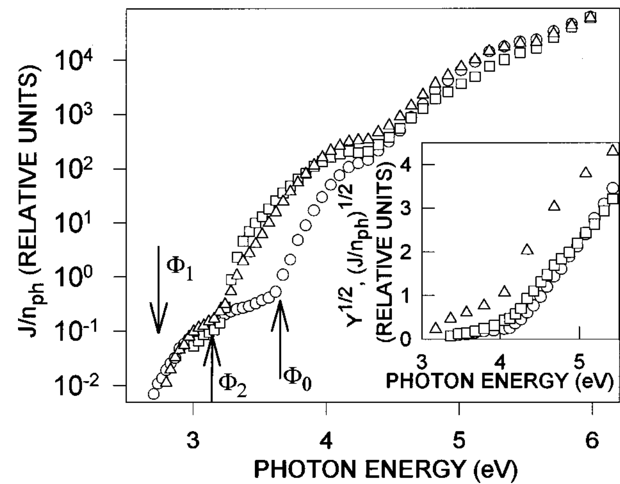

FIG. 6. Photocurrent per incident photon as a function of photon energy in the control Si/SiO_2(66 nm)/Al structure (○), after additional exposure to 1×10^{19} 10-eV photons cm^{-2} without (□) and with subsequent H_2 anneal at 400 °C (△) measured at the electric-field strength in the oxide of 4 MV/cm under positive metal bias. The arrows mark the spectral thresholds. The insert shows spectral characteristics of photocurrent measured at $F = 1$ MV/cm with the metal biased positively (○) and negatively (□), and the quantum yield of PN measured at $F = 3$ MV/cm (metal positively biased) (△) for the irradiated H_2-annealed samples after trapping 6×10^{12} electrons/cm^2 in the bulk of the oxide.

to the electron emission from oxide defects near the Si/SiO_2 interface. As apparent from the data, the irradiation has little effect on the electron emission from these centers. However, the 10-eV irradiation is seen to lead to the development of a new band, characterized by $Y \sim (h\nu - \Phi_2)^2$ and the field-independent spectral threshold $\Phi_2 = (3.1 \pm 0.1)$ eV. We found this emission gradually increasing with irradiation of the oxide, and therefore, this band is associated with radiation-induced defects near the Si/SiO_2 interface. Subsequent annealing in H_2 of the irradiated sample causes a weak, though distinguishable spectral redistribution of the quantum yield in this band (see Fig. 6) but does not eliminate it, while no ESR-active E'_γ centers remain in the SiO_2 after this anneal, and the density of Si/SiO_2 interface states is found reduced by about an order of magnitude as compared to the as-irradiated sample. Probably then, the optical activity of the H-complexed O vacancy is related to the localization of an electron at the ($O_3\equiv SiH$) fragment.

The insert in Fig. 6 shows the PN yield curve and two curves of photocurrent per incident photon measured after electron injection into the irradiated and hydrogenated sample, leading to the buildup of negative charge to a density of 6×10^{12} el./cm^2 in the bulk of the oxide. The curves indicate two spectral thresholds of the electron detrapping, i.e., at (3.1 ± 0.2) and (4.3 ± 0.2) eV. Obviously, the first threshold corresponds to the Φ_2 value determined above for the defects generated near the Si/SiO_2 interface as particularly evidenced by the fact that the same power law of the spectral curve $Y \sim (h\nu - \Phi_2)^2$ is observed in both cases. Apparently, the hydrogenated oxygen vacancy may account for the PN band at $h\nu > 3.1$ eV. The 4.3-eV feature on the photocurrent curves in Fig. 6 may be partially related to the well-known optical reflection peak from crystalline Si.[33] However, the

same threshold on the PN yield curve (see insert) refers to a charge variation associated with Si particles. Therefore, it is concluded that there exists an additional PN threshold at ~4.3 eV.

IV. DISCUSSION

A. Origin of the PI/PN DOS

A most remarkable result of the present study is the nearly identical PI/PN DOS energy distribution in samples with a different average size of Si particles (cf. Figs. 4 and 5), implying that the transitions from neutral and negative states (states corresponding to a different number of electrons in the Si particle) occur by optical excitation of energetically indistinguishable states. This conclusion may be strengthened further by taking into account that the observed 200–300 meV shift of the PI DOS with respect to PN DOS is probably related to the different charge state of the excited particle: During PI, the electron interacts with the hole left at the Si particle; the simple Coulomb interaction with a charge of opposite sign positioned at distance r_c will shift the electron energy by 50–250 meV for the r_c values listed in Table I, when taking the relative permittivity equal to that of Si ($\varepsilon_{Si}=11.8$, Ref. 33). Obviously, this contribution must be absent in PN because the excited electron leaves a neutral particle. Therefore, the experiments show that the occupied highest electron state involved in optical excitation has the same energy (within an accuracy of, say, 200 meV) in a neutral Si particle and in that with an added electron (negatively charged).

The latter conclusion contradicts the simple picture of excitation of a Si cluster based on an electronic spectrum modified by quantum confinement:[4,50] in this case the energy splitting between the highest occupied states in a neutral and negatively charged cluster is expected to be close to the band-gap width and should increase with shrinking cluster size, starting from the bulk Si value [$E_g(\mathrm{Si})=1.12$ eV at 300 K, Ref. 33] onward. Apparently, this is observed only in the nonhydrogenated samples D [cf. Fig. 4(d)]. Therefore, we considered alternative explanations. First, small Si clusters exhibit a considerable reduction in the energy splitting between the highest occupied and the lowest unoccupied state if atomic relaxation of the cluster is allowed. This conclusion is based on theoretical DOS calculations[77] in comparison with photoelectron spectroscopy data for negatively charged *free* Si clusters (Si_n^- , $n\leqslant 12$), some of which show a splitting of only ~0.5 eV.[78] However, this explanation is excluded for several reasons: (i) Only clusters with large splitting are expected to be thermodynamically stable,[77,78] a significant fact in the light of the high-temperature (~1350 °C) annealing used for the presently studied samples; (ii) Both the optical and electrical measurements reveal the porous Si band gap to be 2–2.5 eV,[31,32,79,80] i.e., clusters with smaller gaps are insignificant already at room temperature; (iii) The spectroscopic ellipsometry of samples of types $A-C$ typically reveals the presence of inclusions with dielectric response similar to that of Si—crystalline or amorphous[81,82]—exhibiting an $E_g>1$ eV.

Second, one might refer to the possible influence of donor centers in the Si particles, i.e., if the Si particles were of n type, the PI and PN energies would be close. This hypothesis, however, is also discarded as no difference is observed between the samples prepared on n- and p-type Si substrates. Moreover, the ESR measurements at 4.3 K, highly sensitive to unpaired electrons on donor centers, show no presence of such states in the as-fabricated samples. Thus, the possible influence of donor centers produced during postimplantation annealing can be excluded.

Third, the favored alternative explanation for the coinciding PI and PN DOS distributions is that both processes occur by optical excitation of an electron from the energetically lowest localized state in the Si particle or in the interfacial SiO_2 layer of the Si particle/SiO_2 system, which will be filled upon trapping the additional electron. The same may be true when an electron-hole pair is optically generated in the Si particle: if the mean time for trapping is shorter than for recombination, the generated electron will be transferred to the localized state. In this way the same state may be filled both when starting from negatively charged and neutral particles, and, if its lifetime is long enough, a similar DOS for PI and PN will be observed.

The distinction between the states originating form the Si particle itself and from the surrounding oxide can be made on the basis of their behavior upon hydrogenation. The long experience of Si electronic device technology and the a-Si:H studies clearly show that the primary effect of H consists in passivation of defect states, which removes the corresponding defect levels from the Si band gap. However, the trends observed in the PN/PI DOS are just opposite: The hydrogenation shifts the 3.5-eV DOS band within the Si band gap, as most prominently shown by the results for sample D in Fig. 5(c). The effect can be easily explained by modification of defects by hydrogen in the oxide surrounding the Si particles. The buried SiO_2 layers used in the present work are well known to exhibit a strong H uptake[83] which leads to intense generation of E'_γ centers upon subsequent irradiation.[84–86] The sensibilization to E'_γ center generation is ascribed to the formation of $O_3\equiv SiH$ fragments upon H_2 annealing, which were shown to provide trapping sites for electrons at $E_C(SiO_2)-E_t=3.1$ eV (see Sec. III C). This picture agrees with the presently observed shift of the DOS distribution to higher $E=E_C(SiO_2)-E_t$ values (Fig. 5). In contrast, these effects cannot be explained by modification of the electronic spectrum of bulk Si, e.g., the SiO_2 layers formed in ultradry O_2 and pyrogenic H_2O are found to show no difference in the Si/SiO_2 band offsets within an accuracy of 30 meV. The suggested optical excitation from oxide defects is supported by two other important observations: (i) The energy of the oxide trap should be insensitive to the electronic spectrum of the Si particle, i.e., no size effect should be observed. The latter is evident from the experimental results (cf. Figs. 4 and 5); (ii) The energy onset of the PN DOS matches with the energy of the oxide centers discussed in Sec. III C. Therefore, we conclude that the upper (3.5 eV) band in the PI/PN DOS corresponds to the energy spectrum of the near-interfacial oxide defects—apparently of two different types—that trap electrons photoexcited inside the Si particles or supplied additionally from the oxide. Only part of the 4.5 eV DOS bands—exhibiting a reduced sensitivity to H—may be associated with valence states of a Si particle.

The trap mediated PI/PN mechanism explains consistently the important trends observed in the DOS. Obviously, at least one defect state has to be located in the oxide surrounding the Si particle so as to provide the necessary electron state. If the particles are small, however, there is enhanced probability to find some with no defects in their vicinity. They will then exhibit the DOS corresponding to the intrinsic electronic spectrum of the Si particle. Indeed, in samples type *D*, the PN DOS shown in Figs. 4(d) and 5(c) reveals a shallow component at $E=E_C(\mathrm{SiO_2})-E_t\sim2$ eV, probably related to the quantum confinement of electrons in the Si particle conduction band. This also agrees with the attendant increase of the PI DOS band at ~4.5 eV relative to the band at 3.5 eV (Fig. 4). A remarkable observation here is that the splitting between these bands (~2.5 eV) is close to the range of the band gap width values reported for porous Si and attributed there to the influence of quantum confinement.[79,80] When the density of defects is increased upon hydrogenation, the shallow PN band disappears, as shown in Fig. 5(c), while the defect-related band at ~3.5 eV is significantly enhanced. Similarly, the PI of small particles appears only possible in the UV range [cf. Fig. 4(d)], which is ascribed to the absence of oxide defects that may serve as intermediate excited states for the 3.5-eV PI band.

A most interesting question, definitely, concerns the atomic nature of the defects states revealed by PI and PN. The one with energy level at $E_C(\mathrm{SiO_2})-E_t=3.1$ eV (see Fig. 6) can be convincingly related to the hydrogenated O vacancy ($O_3\equiv$Si-H complex), as discussed in Sec. III C. Regarding the second state, at $E_C(\mathrm{SiO_2})-E_t=2.8$ eV, revealed by PST, we notice that it is diamagnetic when neutral, it correlates with Si enrichment of the oxide, and is stable against interaction with H. This suggests this energy level to belong to a saturated bonding configuration of an excess Si atom. The choice is narrowed down to two types of bonds: Si-Si and Si-H. The latter configuration looks favorable in view of the close energy level of trapped electrons (3.1 eV), and close photoionization cross section (see Sec. III B). However, there is one experimental observation, namely, the absence of a PST signal from these 3.1-eV states, which may be indicative for a different defect structure: The PST probability is proportional to the lifetime of the excited state, and the fact that it is strongly decreased may refer to an additional mechanism of energy dissipation, e.g., a different electronic/vibrational spectrum of the defect. At the same time, we observe a significant difference between the energy level measured in the present study and that [~1 eV below $E_C(\mathrm{SiO_2})$] predicted by theoretical calculations for the oxygen vacancy in $\mathrm{SiO_2}$.[27,28] For this, however, there is the option that the Si-Si distance R may be much less than that used for the Feigl-Fowler-Yip model in Ref. 28 ($R=2.9$ Å). This would lead to an increase of the local positive charge related to the shift of the electron density from Si to the backbonding O atoms, and accordingly to a deeper energy level for a trapped electron. We believe that distinction between these two models of the 2.8-eV defect can be made on the basis of ESR analysis, in which the H-related state would give rise to a proton hyperfine doublet.

B. Luminescence of Si particles in $\mathrm{SiO_2}$ in the perspective of PI/PN DOS

From the inferred DOS distributions corresponding to optical excitation of Si particles in $\mathrm{SiO_2}$ (Figs. 4,5) one may estimate the energies of the electronic transitions which, if radiative, could give luminescence. First, the transitions between two bands in the DOS would have an energy in the range 1.2–1.7 eV. This range overlaps with the PL band from the confined exciton states in Si nanocrystals centered at 1.72 eV,[12–14,87] which would result in spectral redistribution of the PL. However, because the red luminescence from our samples was not analyzed, it is difficult to discuss the corresponding variations of the PL spectra. Moreover, if these transitions in the oxide would appear nonradiative they would quench PL rather than produce an additional band.

Second, the electron excitation from the populated 3.5 eV DOS band to shallow levels below the oxide conduction band may result in transitions at higher energy. The PN DOS and the yield spectra show that the highest occupied energy levels (negatively charged state) are situated at 2.8 and 3.1 eV below $E_C(\mathrm{SiO_2})$. The excited states of the defects are expected to be situated just below the conduction band of the oxide. At least for the 2.8 eV center, the PST reveals the presence of such excited states in the range 0.05–0.4 eV below $E_C(\mathrm{SiO_2})$.[73] Therefore, blue PL (2.4–2.8 eV) might be expected provided there is a radiative decay channel. The existence of such channel is supported by the observation that the blue EL is strongly enhanced by the presence of Si particles (Sec. II A).

Regarding the 3.1-eV defects, they may probably provide PL in a close spectral range. In addition, the latter defect has a second energy level at $E_C(\mathrm{SiO_2})-E_t=4.3$ eV, as suggested by the PN yield spectra. Then, upon excitation of an electron from this state, two radiative transitions are possible: the blue one (from the excited state near $E_C(\mathrm{SiO_2})$ to the empty 3.1-eV level), and the UV band (transition from the excited state near $E_C(\mathrm{SiO_2})$ to a hole left at the 4.3-eV level). The characteristic feature of these transitions is that they require no tunneling of a hole; therefore, the PL decay may be expected to be fast. The UV PL, indeed, shows decay times in the ns range.[1,3,5,8,49,88] By contrast, the blue PL has two components with the decay times differing by many orders of magnitude: from the ns range in oxidized porous Si [Refs. 3,5,6,38,42,45] to the 10^{-2}-s range in bulk $\mathrm{SiO_2}$.[15–17] This huge difference between the fast and slow PL components may potentially also be explained within the present model by taking into account the different lifetimes of the excited state for the two defects revealed in the present study by PST, and the possibility of electron tunneling from an excited state back to the Si particle, which is absent in bulk $\mathrm{SiO_2}$. We would like to mention here that the PL excitation peaks observed for the blue PL at ~3 and ~4.3 eV [Refs. 89–91] are consistent with the here proposed optical excitation of the electron states contributing to the PN DOS. Finally, it is worth pointing out that, despite of the invoked charge transfer to the defect state, the PL efficiency may remain sufficiently high: Using the value $\sigma_{\mathrm{ph}}=1\times10^{-18}$ cm^2 inferred from PN experiments (Sec. III B), the observed efficiency of blue PL in the thermally oxidized porous Si of 0.1% (Ref. 3) would require a density of charged defects of $\sim10^{15}$ cm^{-2}. This, however, is certainly realistic taking into account the long lifetime of the trapped electron at the defect sites, the large thicknesses of the oxidized porous Si layers (>10 μm),[14] and the tremendous area of in-

ternal Si/SiO_2 interfaces, which may be 10^3 times enhanced over the planar surface. Worthy of notice here is that the system remains neutral because upon electron transfer to the oxide defect the hole remains at the Si particle, i.e., no Coulomb blockage of the globally proceeding charge transfer is expected.[92]

The comparison between the short-wavelength PL properties and the DOS of Si particles in SiO_2 may be extended further by analyzing the multicomponent nature of the green-blue PL bands and their spectral width, the relation of size effects to the broad energy distribution of the states involved, the influence of temperature, effects of hydrogen, etc. We are convinced, however, that only the direct correlative analysis of the PL and the PI/PN DOS may establish the firm relationship between particular defects and the PL bands. In this view, the above presented interpretation of PL has to be considered only as a suggestion for the physical mechanism of PL, in addition to PL of the quantum-confined exciton states, observed from the system composed of Si particles surrounded by SiO_2.

V. CONCLUSIONS

The analysis of photoionization and photoneutralization of small Si particles in SiO_2 importantly reveals that both the optically generated or externally supplied electrons are trapped by oxide defects situated at the Si particle/oxide interface. The spectrum of the oxide traps is sensitive to hydrogenation, and two oxide defects with energy levels in the required range are isolated. One of them is related to Si enrichment of the oxide and has the energy level of the negatively charged state at 2.8 eV below the oxide conduction band; Another defect, characterized as a H-complexed oxygen vacancy in SiO_2, has the energy level of an additionally trapped electron at 3.1 eV below $E_C(SiO_2)$. Comparison of the inferred density of states distribution and the photoluminescence data available in the literature suggests the mechanism of PL mediated by electron trapping at oxide imperfections as a feasible explanation of the luminescent properties of oxidized Si particles in the green-blue and UV spectral ranges.

ACKNOWLEDGMENTS

The authors are grateful to A. G. Revesz (Revesz Associates, Bethesda, MD) and to H. L. Hughes (Naval Research Laboratory, Washington, D.C.) for providing samples. Particular thanks are due to A. G. Revesz for providing the unpublished EL data and for stimulating discussions.

[1] V. Petrova-Koch, T. Muschik, A. Kux, B. K. Meyer, F. Koch, and V. Lehmann, Appl. Phys. Lett. **61**, 943 (1992).
[2] J. C. Vial, A. Bsiesy, F. Gaspard, R. Herino, M. Ligeon, F. Muller, R. Romestain, and R. M. McFarlane, Phys. Rev. B **45**, 14 171 (1992).
[3] L. Tsybeskov, Ju. V. Vandyshev, and P. M. Fauchet, Phys. Rev. B **49**, 7821 (1994).
[4] R. T. Collins, P. M. Fauchet, and M. A. Tischler, Phys. Today **50**(1), 24 (1997).
[5] D. I. Kovalev, I. D. Yaroshetzkii, T. Muschik, V. Petrova-Koch, and F. Koch, Appl. Phys. Lett. **64**, 214 (1994).
[6] Y. Kanemitsu, T. Futagi, T. Matsumoto, and H. Mimura, Phys. Rev. B **49**, 14 732 (1994).
[7] A. J. Kontkiewicz, A. M. Kontkiewicz, J. Siejka, S. Sen, G. Nowak, A. M. Hoff, P. Sakthivel, K. Ahmed, P. Mukherjee, S. Witanachchi, and J. Lagowski, Appl. Phys. Lett. **65**, 1436 (1994).
[8] L. H. Dinh, L. L. Chase, M. Balooch, L. J. Terminello, and F. Wooten, Appl. Phys. Lett. **65**, 3111 (1994).
[9] D. T. Jiang, I. Coulthard, T. K. Sham, J. W. Lorimer, S. P. Frigo, X. H. Feng, and R. A. Rosenberg, J. Appl. Phys. **74**, 6335 (1993).
[10] J. Lin, G. Q. Yao, J. Q. Duan, and G. G. Qin, Solid State Commun. **97**, 221 (1996).
[11] G. G. Qin, J. Lin, J. Q. Duan, and G. Q. Yao, Appl. Phys. Lett. **69**, 1689 (1996).
[12] L. T. Canham, Appl. Phys. Lett. **57**, 1046 (1990).
[13] A. G. Cullis, L. T. Canham, G. M. Williams, P. W. Smith, and O. D. Dosser, J. Appl. Phys. **75**, 493 (1994).
[14] A. G. Cullis, L. T. Canham, and P. D. J. Calcott, J. Appl. Phys. **82**, 909 (1997).
[15] J. H. Stathis and M. A. Kastner, Phys. Rev. B **35**, 2972 (1987).
[16] R. Tohmon, Y. Shimogaichi, H. Mizuno, Y. Ohki, K. Nagasawa, and Y. Hama, Phys. Rev. Lett. **62**, 1388 (1989).
[17] C. Itoh, T. Suzuki, and N. Itoh, Phys. Rev. B **41**, 3794 (1990).
[18] A. N. Trukhin, L. N. Skuja, A. G. Bogdanov, and V. S. Rudenko, J. Non-Cryst. Solids **149**, 96 (1992).
[19] N. Kuzuu and M. Murahara, Phys. Rev. B **47**, 3083 (1993).
[20] R. Tohmon, H. Mizuno, Y. Ohki, K. Sasagane, K. Nagasawa, and Y. Hama, Phys. Rev. B **39**, 1337 (1989).
[21] H. Nishikawa, T. Shiroyama, R. Nakamura, Y. Ohki, K. Nagasawa, and Y. Hama, Phys. Rev. B **45**, 586 (1992).
[22] H. Nishikawa, E. Watanabe, D. Ito, M. Takiyama, A. Ieki, and Y. Ohki, J. Appl. Phys. **78**, 842 (1995).
[23] H. Nishikawa, E. Watanabe, D. Ito, Y. Sakurai, K. Nagasawa, and Y. Ohki, J. Appl. Phys. **80**, 3513 (1996).
[24] L. Skuja, J. Non-Cryst. Solids **149**, 77 (1992).
[25] V. Petrova-Koch, T. Muschik, D. I. Kovalev, F. Koch, and V. Lehmann, in *Microcrystalline Semiconductors: Materials Science & Devices*, edited by P. M. Fauchet, C. C. Tsai, L. T. Canham, I. Shimizu, and Y. Aoyagi, MRS Symposia Proceedings No. 283 (Materials Research Society, Pittsburgh, 1993), p. 178.
[26] F. Koch, in *Silicon-Based Optoelectronic Materials*, edited by M. A. Tischler, R. T. Collins, M. L. Thewalt, and G. Absteriter, MRS Symposia Proceedings No. 298 (Materals Research Society, Pittsburgh, 1993), p. 319, Microelectron. Eng. **28**, 237 (1995).
[27] J. K. Rudra and W. B. Fowler, Phys. Rev. B **35**, 8223 (1987).
[28] A. X. Chu and W. B. Fowler, Phys. Rev. B **41**, 5061 (1990).
[29] E. M. Dianov, V. O. Sokolov, and V. B. Sulimov, J. Non-Cryst. Solids **149**, 5 (1992).
[30] A. M. Goodman, Phys. Rev. **152**, 720 (1966).
[31] V. Lehmann and U. Gösele, Appl. Phys. Lett. **58**, 856 (1991).
[32] Y. Kanemitsu, H. Uto, Y. Matsumoto, T. Matsumoto, T. Futagi, and H. Mimura, Phys. Rev. B **48**, 2827 (1993).

[33] S. M. Sze, *Physics of Sermiconductor Devices*, 2nd ed. (Wiley, New York, 1981).
[34] S. M. Prokes and O. J. Glembocki, Phys. Rev. B **49**, 2238 (1994).
[35] J. L. Gole, F. P. Dudel, D. Grantier, and D. A. Dixon, Phys. Rev. B **56**, 2137 (1997).
[36] Y. Kanemitsu, S. Okamoto, M. Otobe, and S. Oda, Phys. Rev. B **55**, R7375 (1997).
[37] S. Komuro, T. Kato, T. Morikawa, P. O'Keeffe, and Y. Aoyage, Appl. Phys. Lett. **68**, 949 (1996).
[38] X. Zhao, O. Schoenfeld, S. Komuro, Y. Aoyagi, and T. Sugano, Phys. Rev. B **50**, 18 654 (1994).
[39] P. N. Saeta and A. C. Gallagher, Phys. Rev. B **55**, 4563 (1997).
[40] T. Shimizu-Iwayama, S. Nakao, and K. Saitoh, Appl. Phys. Lett. **65**, 1814 (1994).
[41] P. Mutti, G. Ghislotti, S. Bertoni, L. Bondoli, G. F. Cerofolini, L. Meda, E. Grilli, and M. Guzzi, Appl. Phys. Lett. **66**, 851 (1995).
[42] L.-S. Liao, X.-M. Bao, X.-Q. Zheng, N.-S. Li, and N.-B. Min, Appl. Phys. Lett. **68**, 850 (1996).
[43] G. Ghislotti, B. Nielsen, P. Asoka-Kumar, K. G. Lynn, A. Gambhir, L. F. DiMauro, and C. E. Bottani, J. Appl. Phys. **79**, 8660 (1996).
[44] K. S. Min, K. V. Shcheglov, C. M. Yang, H. A. Atwater, M. L. Brongersma, and A. Polman, Appl. Phys. Lett. **69**, 2033 (1996).
[45] A. Pifferi, P. Taroni, A. Torricelli, G. Valentini, P. Mutti, G. Ghislotti, and L. Zanghieri, Appl. Phys. Lett. **70**, 348 (1997).
[46] E. Neufeld, S. Wang, R. Apetz, Ch. Buchal, R. Carius, C. W. White, and D. K. Thomas, Thin Solid Films **294**, 238 (1997).
[47] S. I. Fedoseenko, V. K. Adamchuk, and V. V. Afanas'ev, Microelectron. Eng. **22**, 367 (1993).
[48] S. Bota, A. Perez-Rodrigues, J. R. Morante, A. Baraban, and P. P. Konorov, in *Silicon-on-Insulator Technology and Devices*, edited by S. Cristoloveanu, K. Izumi, P. L. F. Hemment, and H. Hosack, Electrochemical Society Proceedings Vol. 94-11 (Electrochemical Society, Inc., Pennington, 1994), p. 179.
[49] K. S. Seol, A. Ieki, Y. Ohki, H. Nishikawa, and M. Tachimori, J. Appl. Phys. **79**, 412 (1996).
[50] D. J. DiMaria, J. R. Kirtley, E. J. Pakulis, D. W. Dong, T. S. Kuan, F. L. Pesavento, T. N. Theis, J. A. Cutro, and S. D. Brorson, J. Appl. Phys. **56**, 401 (1984).
[51] A. J. Kenyon, P. F. Trwoga, C. W. Pitt, and G. Rehm, J. Appl. Phys. **79**, 9291 (1996).
[52] K. Kim, M. S. Suh, T. S. Kim, C. J. Youn, E. K. Suh, Y. J. Shin, K. B. Lee, H. J. Lee, M. H. An, H. J. Lee, and H. Ryu, Appl. Phys. Lett. **69**, 3908 (1996).
[53] Y. Kanazawa, S. Hayashi, and K. Yamamoto, J. Phys.: Condens. Matter **8**, 4823 (1996).
[54] Y. Kanazawa, T. Kageyama, S. Takeoka, M. Fujii, S. Hayashi, and K. Yamamoto, Solid State Commun. **102**, 533 (1997).
[55] Y. Ishikawa, N. Shibata, and S. Fukatsu, Thin Solid Films **294**, 227 (1997).
[56] A. G. Revesz, G. A. Brown, and H. L. Hughes, J. Electrochem. Soc. **140**, 3222 (1993).
[57] V. V. Afanas'ev, G. A. Brown, H. L. Hughes, S. T. Liu, and A. G. Revesz, J. Electrochem. Soc. **143**, 347 (1996).
[58] V. V. Afanas'ev, A. Stesmans, A. G. Revesz, and H. L. Hughes, J. Appl. Phys. **82**, 2184 (1997).
[59] V. V. Afanas'ev, A. Stesmans, and M. E. Twigg, Phys. Rev. Lett. **77**, 4206 (1996).
[60] A. G. Revesz (private communication).
[61] V. V. Afanas'ev, J. M. M. de Nijs, P. Balk, and A. Stesmans, J. Appl. Phys. **78**, 6481 (1995).
[62] J. H. Thomas, III and F. J. Feigl, Solid State Commun. **8**, 1669 (1970).
[63] D. A. Mehta, S. R. Butler, and F. J. Feigl, J. Appl. Phys. **43**, 4631 (1972).
[64] D. J. DiMaria, F. J. Feigl, and S. R. Butler, Phys. Rev. B **11**, 5023 (1975).
[65] V. J. Kapoor, F. J. Feigl, and S. R. Butler, J. Appl. Phys. **48**, 739 (1977).
[66] G. Lucovsky, Solid State Commun. **3**, 299 (1965).
[67] P. T. Landsberg, *Recombination in Semiconductors* (University Press, Cambridge, 1991), p. 389.
[68] V. V. Afanas'ev, A. Stesmans, and M. O. Andersson, Phys. Rev. B **54**, 10 820 (1996).
[69] T. H. Ning and H. Y. Yu, J. Appl. Phys. **45**, 5373 (1974).
[70] V. V. Afanas'ev, A. G. Revesz, and H. L. Hughes, J. Electrochem. Soc. **143**, 695 (1996).
[71] C. N. Berglund and R. J. Powell, J. Appl. Phys. **42**, 573 (1971).
[72] C. Sebenne, D. Bolmont, G. Guichar, and M. Balkanski, Phys. Rev. B **12**, 3280 (1975).
[73] V. V. Afanas'ev and A. Stesmans, Phys. Rev. Lett. **78**, 2437 (1997).
[74] V. V. Afanas'ev and A. Stesmans, Appl. Phys. Lett. **70**, 1260 (1997).
[75] V. V. Afanas'ev and A. Stesmans, Microelectron. Eng. **36**, 149 (1997).
[76] R. Williams, Phys. Rev. **140**, A569 (1965).
[77] N. Binggeli and J. R. Chelikowsky, Phys. Rev. Lett. **75**, 493 (1995).
[78] O. Cheshnovsky, S. H. Yang, C. L. Pettiette, M. J. Craycraft, Y. Liu, and R. E. Smalley, Chem. Phys. Lett. **138**, 119 (1987).
[79] Z. Chen, T.-Y. Lee, and G. Bosman, Appl. Phys. Lett. **64**, 3446 (1994).
[80] L. Burstein, Y. Shapira, J. Patree, J. Shinar, Y. Lubianiker, and I. Balberg, Phys. Rev. B **55**, R1930 (1997).
[81] B. J. Mrstik, P. J. McMarr, R. K. Lawrence, and H. L. Hughes, IEEE Trans. Nucl. Sci. **41**, 2277 (1994).
[82] M. J. Anc, L. P. Allen, R. P. Dolan, B. F. Cordts, G. Ryding, M. A. Mendicino, X. Shi, W. Mazara, R. Dockerty, P. K. Vasudev, and P. Roitman, in *Proceedings of 1996 IEEE International SOI Conference* (IEEE, Piscataway, 1996), p. 54.
[83] S. M. Myers, G. A. Brown, A. G. Revesz, and H. L. Hughes, J. Appl. Phys. **73**, 2196 (1993).
[84] R. A. B. Devine, J.-L. Leray, and J. Margail, Appl. Phys. Lett. **59**, 2275 (1991).
[85] D. Herve, J.-L. Leray, and R. A. B. Devine, J. Appl. Phys. **72**, 3634 (1992).
[86] M. E. Zvanut, R. E. Stahlbush, W. E. Carlos, R. K. Lawrence, R. Hevey, and G. A. Brown, IEEE Trans. Nucl. Sci. **38**, 1253 (1991).
[87] P. D. J. Calcott, K. J. Nash, L. T. Canham, M. J. Kane, and D. Brumhead, J. Lumin. **57**, 257 (1993).
[88] K. S. Seol, Y. Ohki, H. Nishikawa, M. Takiyama, and Y. Hama, J. Appl. Phys. **80**, 6444 (1996).
[89] A. Kux, D. Kovalev, and F. Koch, Appl. Phys. Lett. **66**, 49 (1995).
[90] H. Z. Song and X. M. Bao, Phys. Rev. B **55**, 6988 (1997).
[91] G. G. Qin, X. S. Liu, S. Y. Ma, J. Lin, G. Q. Yao, X. Y. Lin, and K. X. Lin, Phys. Rev. B **55**, 12 876 (1997).
[92] V. V. Afanas'ev and V. K. Adamchuk, Prog. Surf. Sci. **47**, 301 (1994).